Marine Geology 346 (2013) 256–261

Contents lists available at ScienceDirect

Marine Geology

journal homepage: www.elsevier.com/locate/margeo

Letter

A technique for estimation of suspended sediment concentration in very high turbid coastal waters: An investigation from Gulf of Cambay, India

D. Ramakrishnan *, Rishikesh Bharti, M. Das

Department of Earth Sciences, Indian Institute of Technology Bombay, Mumbai 400076, India

ARTICLE INFO

Article history:
Received 18 June 2013
Received in revised form 29 September 2013
Accepted 7 October 2013
Available online 15 October 2013

Communicated by J.T. Wells

Keywords:
suspended sediment concentration
ocean color monitor
coastal waters
Gulf of Cambay

ABSTRACT

This paper presents a technique to estimate the suspended sediment concentration (SSC) in Case-2 waters based on spectral similarity between satellite images and library spectra. Average Weighted Spectral Similarity (AWSS), a measure of spectral matching, is used to estimate SSC ranges in ocean color monitor (OCM) data of Gulf of Cambay (GC), India. For this, a spectral library comprising field and laboratory measured data representing diverse sediment mineralogy and grain sizes was generated. Results estimated by AWSS were compared with other published procedures and observed to be more accurate ($R^2 = 0.95$ at 99% significance). Further, in Case-2 waters reflectance in bands centered at 743 and 835 nm is more sensitive to SSC changes. Sediment concentration and grain size significantly affect reflectance of water.

© 2013 Elsevier B.V. All rights reserved.

1. Introduction

Understanding the distribution and movement of SSC is necessary in addressing many coastal problems such as siltation of ports, modification of coastal morphology, scouring, and variation of underwater topography. Spatial data on SSC collected by field-based techniques are often spatially limited and the procedures involved in collecting such data are tedious and costly. Satellite data in conjunction with quasi-synchronous field data such as reflectance, Secchi disk compensation depth, and turbidity have been extensively used for successful estimation of sediment flux and its dispersion (Doerffer and Fischer, 1994; Forget and Ouillon, 1998). These procedures require elaborate field and laboratory analyses to estimate the SSC and are therefore better suited for microscale applications.

However in recent studies, interrelationship between sediment concentration and spectral reflectance of water is proven to be an easy, cost effective and accurate alternative for estimating the SSC (Dekker et al., 2001; Doxaran et al., 2002; Deng and Li, 2003; Miller and McKee, 2004; Han et al., 2006; Chen et al., 2007). This understanding led to the development of inversion algorithms based on the interrelationship between SSC and spectral reflectance with measurements ranging from laboratory to satellite scales (Lira et al., 1997; Miller and McKee, 2004). Though satellite based estimates are advantageous, adequate care is necessary to calibrate satellite-reflectance with field measurements (Chauhan et al., 2005; Kunte, 2008). This requires an efficient SSC retrieval algorithm and good understanding of vital reflectance-influencing parameters such as angular distribution of light, mineralogy, grain size, abundance of organic detritus, and phytoplankton (Yanjiao et al., 2007). Prevailing retrieval algorithms can be broadly grouped into three major categories such as empirical based (Tassan, 1993; Deng and Li, 2003; Miller and McKee, 2004; Han et al., 2006; Chen et al., 2007), radiative transfer based (Doerffer and Fischer, 1994), and semi-analytical procedure based (Dekker et al., 2001; Doxaran et al., 2002; Warrick et al., 2004).

In this study, we developed a semi-analytical SSC inversion model for very high-turbid waters of the Gulf of Cambay region, India using field, laboratory, and satellite based spectral measurements. The study area is one of the best sites in the world to study reflectance–SSC relationship of very high turbid coastal waters (Nambiar and Rajagopalan, 1995). We used OCM satellite data onboard Indian Remote Sensing Satellite (IRS) P-4 for achieving the above objectives.

2. Study area

The GC is situated between the mainland Gujarat and Saurashtra peninsula in the west coast of India. It is bounded by northern latitudes 21°00′ and 22°16′ and eastern longitudes 72°00′ and 73°00′ and encompasses estuaries of seven major rivers including Sabarmati, Mahi, Dadar, Narmada, Tapti, Ambika and Shetrunji that debouch very high sediment loads (6×10^7 metric tons/year). These rivers discharge a large amount of sediment as suspended load into the Gulf with an average monthly water discharge exceeding 2000 $m^3\ s^{-1}$ (Kunte, 2008). The GC is also known for strong tidal currents with high tides often rising up to 11 m from the normal waterline (Jervis, 1838; Unnikrishnan et al., 1999).

* Corresponding author. Tel.: +91 22 25767255.
E-mail address: ramakrish@iitb.ac.in (D. Ramakrishnan).

0025-3227/$ – see front matter © 2013 Elsevier B.V. All rights reserved.
http://dx.doi.org/10.1016/j.margeo.2013.10.001

3. Materials and methods

3.1. Field data collection

A field cruise was carried out between 26th and 30th of December, 2006 in the GC and estuaries of Mahi, Narmada, and Purna with an aim to obtain spectral reflectance, water and sediment-samples, and Secchi disk compensation depth. Acid-leached 1000 mL Teflon bottles were lowered into the water to 20 cm sampling depth, allowed to fill, retrieved, capped tightly, and packed for further analysis. Samples from the fresh mudflats and sand bars (representing the suspended and saltation sediment loads) were collected for mineralogical and additional laboratory based studies on water leaving reflectance. Since the light does not penetrate beyond 4 cm in all cases, in situ above water surface reflectance was collected using GER 1500 field spectroradiometer following the procedures of Doxaran et al. (2002). The reflectance spectra were collected between 10 a.m. and 2 p.m. with nadir looking sensor setup to minimize the adverse effects of geometry (Novo et al., 1989) and glint (Mobley, 1999). In all, 39 spectra and corresponding number of sediment samples were collected with GPS co-ordinates.

3.2. Laboratory analyses and spectral library generation

The SSC concentrations were determined by filtering 1000 mL of the collected water samples on pre-weighed 8 μm filter paper. The filter papers were then dried at 100 °C and re-weighed for estimating the sediment concentration. Mineral composition of the filtrates was determined using a Philips (PW2404) X-ray diffractometer with CuKα source. The mineral identification and qualitative abundance estimation were carried out following the method of Carrol (1970). The grain size of samples representing various estuaries and Gulf was carried out by mechanical sieving and laser particle size analysis techniques.

To augment the spectral database, laboratory experiments were conducted in a test tank with similar field of view (FOV) and sun-sensor geometry to acquire spectral information with contiguous increase in sediment concentration. The experimental setup contains an acrylic water tank (of 1 m^3 capacity), a turbo stirrer to maintain the sediments in suspension and a spectroradiometer to measure reflectance. The sediments collected from the field were dried, weighed, sieved, and mixed to match the grain sizes of the suspended sediment load. Irradiance and upwelling radiances were collected with the aid of GER 1500 field portable spectroradiometer and spectralon panel for the wavelength region from 350 to 1050 nm. Using this setup, contiguous reflectance spectra representing the sediment load from 1 ppm to 6000 ppm (at an interval of 500 ppm) were generated and archived as spectral library for each estuary and Gulf separately.

3.3. Image processing and spatial mapping of SSC

In this study, OCM data for 26th December, 2006 was procured from National Remote Sensing Agency (NRSA), India and processed. OCM collects data in eight narrow spectral channels (402–422, 433–453, 480–500, 500–520, 545–565, 660–680, 745–785, 845–885 nm) with spatial resolution of 360 m and radiometric resolution of 12 bits. Prior to retrieval of SSC, the OCM data was corrected for radiometric, geometric, and atmospheric effects. Geometric correction of the data was carried out with the aid of ground control points (GCPs) collected during the field campaign. Conversion of Top of Atmosphere (TOA) radiances to surface reflectance was carried out following the atmospheric correction procedures of Mohan and Chauhan (2003). Spatially coherent noise in the reflectance image was reduced by using the Minimum Noise Fraction (MNF) algorithm (Green et al., 1988).

Subsequently three different approaches, namely, Total Suspended Matter (TSM), Suspended Sediment Matter Retrieval (SSMR), and spectral similarity based AWSS algorithms were used to map SSC. The TSM algorithm (Sathyendranath et al., 1989) creates a large set of remote sensing reflectance (Rrs) values by independently varying the concentration of chlorophyll-a, suspended matter and yellow substance. The exponential relationship between TSM and reflectance (at 555 and 620 nm) (Eqs. (1) and (2)) is used to predict concentrations.

$$\mathrm{Log}(S) = 266.23 \times \mathrm{Rrs}\,555 - 1.025 \text{ for } 1.0 < S\,(\mathrm{mg/L}) < 250 \quad (1)$$

$$\mathrm{Log}(S) = 164.39 \times \mathrm{Rrs}\,620 - 1.13 \text{ for } 1.0 < S\,(\mathrm{mg/L}) < 250 \quad (2)$$

The SSMR (Ramaswamy et al., 2004) uses reflectance band ratios involving 490, 555, and 670 nm regions (Eqs. (3) and (4)).

$$S = 25 \times \exp(2.16 + 0.991 \times \mathrm{LogXs}) \quad (3)$$

where, S is suspended sediment concentration in mg/L and Xs is variable defined as,

$$Xs = [\mathrm{Rrs}(555) + \mathrm{Rrs}(670)] \times [\mathrm{Rrs}(490)/\mathrm{Rrs}(555)] - 1. \quad (4)$$

Ramakrishnan et al. (2012) observed that even SSMR based estimates yielded inaccurate sediment concentrations in GC. It was also evident from our earlier study that in addition to reflectance at 490, 555, and 670 nm, absorption depths at 740 and 835 nm are very sensitive to changes in SSC. Hence, we used a spectral similarity based approach involving all OCM wavelength regions for estimating the SSC. For this purpose, AWSS was derived by scaling the outputs of Spectral Angle Mapper (SAM — Kruse et al., 1993), Spectral Feature Fitting (SFF — Clark et al., 1990), and Binary Encoding (BE — Mazer et al., 1988) into a measure ranging between 0 and 100% and then each weighted by 33% (i.e. equal-weighting). Since AWSS involves similarity estimation between library (reference) and image spectra (target) based on spectral angle of similarity (SAM), continuum-removed fits (SFF), and average correlation fits (BE), the results are expected to be more accurate than the band ratio based approaches. Typically, AWSS score ranges between 0 and 100% corresponding to least and best correlation between image and library spectra. In this study, AWSS scores exceeding 85% were used to classify the satellite imagery.

4. Results

4.1. SSC and spectral reflectance

It is evident from field (Fig. 1a) and laboratory (Fig. 1b and c) spectra that reflectance of water increases at all wavelengths with increase in SSC. Typical reflectance spectra have three distinct peaks in 400–1000 nm region. The first peak is centered at 590 nm, the second at 700 nm, and the third at 810 nm. At lower SSC (<1000 ppm), the spectra have a characteristic plateau in 590–690 nm window. With progressive increase in SSC (1000–4000 ppm), this plateau disappears and at very high concentrations (>4000 ppm), absorption features at 740 and 835 nm are significantly subdued. To understand wavelength dependent reflectance changes, scatter plots between sediment concentration and reflectance in 490, 555, and 670 nm were analyzed. It is observed that reflectance in higher wavelengths has poor correlation ($R^2 = 0.43$–0.63) with SSC. The error in SSC estimates retrieved using reflectance at 490, 555, and 670 nm are ±1235 ppm, ±1062 ppm and ±939 ppm, respectively.

However, spectral absorption features centered at 480, 743 and 835 nm in the convex hull normalized spectra are very sensitive to changes in SSC (R^2 = 0.97–0.99) at high statistical significance (99%) (Fig. 2). The error in SSC estimate using 743 and 835 nm reflectance values is ±477 ppm and ±447 ppm respectively. With increase in SSC, absorption depth at these wavelengths decreases.

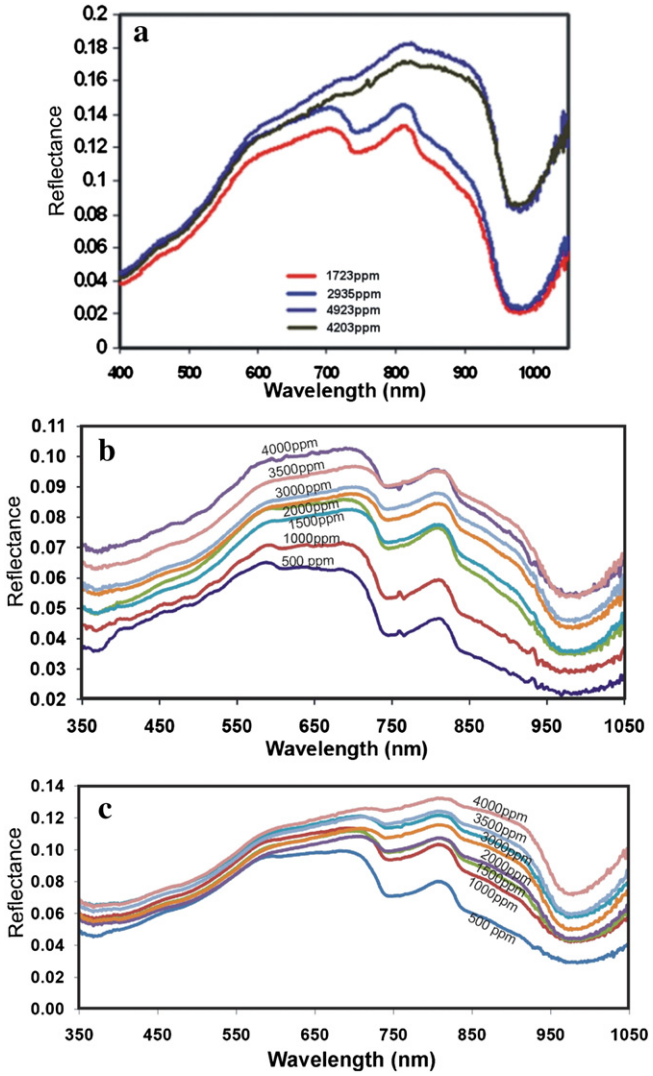

Fig. 1. Reflectance spectra of waters collected from field (a), and laboratory experiments (b — sand), (c — silty-clay) at various SSCs.

The shape of absorption also changes from deep, narrow bandwidth features at lower concentration to shallow and wide feature at higher concentrations. Since atmospheric effects significantly influence 480 nm absorption features, we restricted spectral absorption–SSC relationship analysis to 743 and 835 nm absorption features only.

4.2. Effect of sediment mineralogy and texture on spectral reflectance

Granulometric and XRD results (Table 1) indicate that sediments of estuaries and Gulf vary in grain size and mineralogy. The Mahi estuary is dominated by fine sand and silt size fractions of quartz, mica, orthoclase, and kaolin indicating granitic provenance. The Narmada and Purna estuaries are dominated by clayey-silt sediments of minerals like montmorillonite, calcite, and plagioclase with subordinate amount of quartz, calcite, mica, and kaolinite pointing to basaltic provenance. The latter two estuaries also have higher silt fractions (63–82%) than the Mahi (56–71%). The Gulf sediments, on the other hand, show slightly higher percentage (12–32%) of clay than the estuarine sediments (3–22%) and have minerals such as gypsum, aragonite, and chlorite in addition to the estuarine mineralogy. The organic matter (OM) content of the Gulf is relatively higher (3–3.5%) than the Mahi (2.2–2.4%), Narmada (2.5–3.3%) and Purna (2.9–3.4%) estuaries.

To understand the effect of grain size on reflectance, lab spectra generated using fine- and coarse-sediments (collected from each of the estuaries) were analyzed. For any given sediment concentration, the spectral reflectance of water with fine sediments (Fig. 1c) were slightly higher (2–6%) than with that of coarse sediments (Fig. 1b). It is also evident from Fig. 1 that for a unit increase in SSC, reflectance increase in longer wavelength (650–1000 nm) regions is appreciable compared to the short wavelength regions (350–650 nm).

To evaluate the effect of sediment mineralogy on reflectance, we compared reflectance (at 743 and 865 nm) of waters representing different estuaries and Gulf (Fig. 3). The reflectance scatter plots among Gulf, Mahi and Narmada waters (having similar grain size but differing mineral composition) at various SSCs (Fig. 3a and b) are linear and well correlated ($R^2 = 0.94–0.97$). This relationship is less pronounced when comparison is made with Purna waters (Fig. 3c). This could mainly be attributed to the slightly coarser nature of Purna sediments.

4.3. SSC retrieval using OCM and accuracy assessment

For the analyzed OCM data, SSC ranges estimated by TSM, SSRM, and AWSS algorithms (Fig. 4) are 0–1000 ppm, 0–4000 ppm, and 0–4500 ppm, respectively. Based on the histogram of TSM derived image (Fig. 4a), only two SSC classes (<500 ppm and 500–1000 ppm) could be deciphered. In the classified image, most part of the Gulf (excepting a small portion in the center of the Gulf), falls under a single SSC class (<500 ppm). With the SSRM based approach (Fig. 4b), three distinct ranges of SSC such as 2000–1500 ppm, 1500–1000 ppm, and 1000–500 ppm could be identified. The aerial distribution of above mentioned SSC ranges is 72%, 11%, and 15%, respectively. The SSRM algorithm could also demarcate SSC gradients within the estuaries and Gulf waters (Fig. 4b). However, with this approach lower (<500 ppm) and higher SSC (>2500 ppm) classes could not be resolved. These observations indicate that the chosen reflectance bands (490, 555 and 670 nm) are reasonably sensitive to discriminate SSC changes within certain concentration ranges only.

However, with the AWSS algorithm eleven distinct classes could be identified (Fig. 4c). Some of those classes that were irresolvable with SSMR (<500 ppm and >2500 ppm) could also be discriminated. The aerial distribution of major SSC classes achieved by this algorithm includes 2000–1500 ppm (41%), 1000–500 ppm (32%), <500 ppm (14%), 2000–2500 ppm (3%) and other classes (<10%). Higher resolving power of AWSS permitted discrimination of subtle changes in sediment concentration and helped in identifying low SSC pockets within the high SSC and vice-versa. Further, this approach could also distinctly portray progressive reduction in SSC from the inner Gulf to open ocean.

In this study, accuracy of adopted classification algorithms was statistically evaluated by comparing image derived and field measured SSC values. Since correlations between TSM, SSMR and field measurements are poor for all SSC classes ($R^2 = 0.18–0.47$), accuracy of the AWSS based approach only is detailed here (Table 2). The scatter plots made using AWSS and field measured SSC is linear and shows strong correlation ($R^2 = 0.95$). The F-test aimed at evaluating the strength of statistical relationship indicates that estimated correlation is significant at 99% levels. For most of the samples, the error in SSC estimates varied from 1.7% to 20.3%.

5. Discussion and conclusions

In Case-2 waters, the optical properties of water–sediment mixtures are nonlinear and factors such as particle size, shape and color of sediments have large influences (Pollack and Cuzzi, 1980; Warrick et al., 2004). Conventionally, reflectance in the blue-green and green-red regions (490, 550, 555, 560, 670 nm) is used to estimate the SSC (Tassan, 1993; Ramaswamy et al., 2004; Warrick et al., 2004), which also includes the contributions from Colored Dissolved Organic Matter (CDOM). Where as in this study, SSC is retrieved mainly based

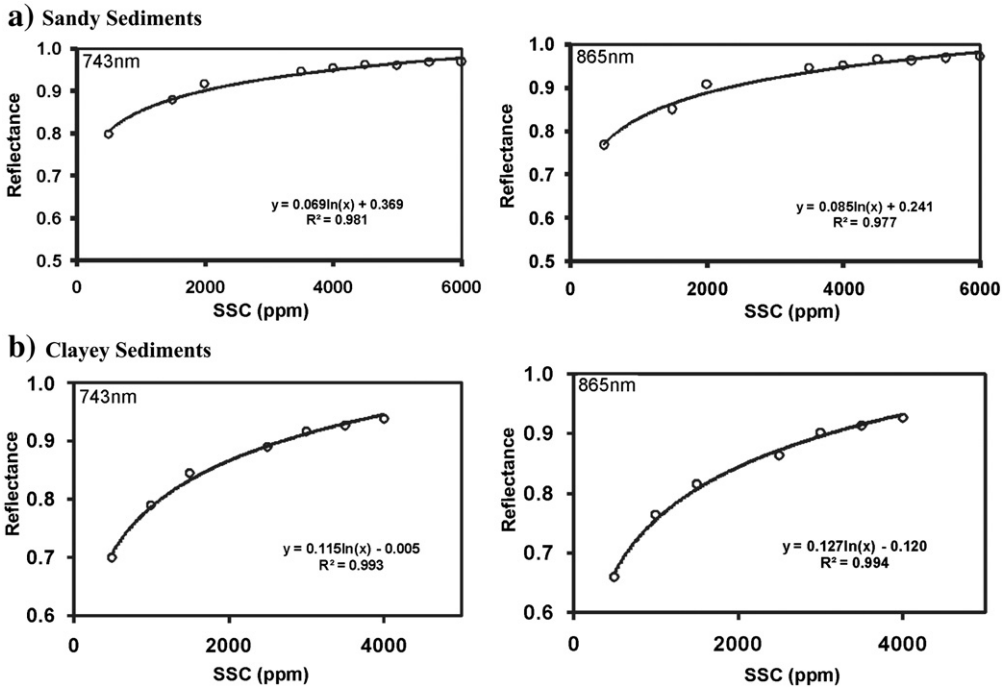

Fig. 2. SSC–reflectance relationship at 743 and 865 nm wavelength for waters with sandy (a) and silty-clay sediments (b).

on spectral absorptions centered at 743 and 835 nm. At these wavelengths, CDOM has no influence and hence, the reflectance can be directly related to SSC. Since reflectance–SSC relationship is complex and non-linear at high sediment concentrations (Warrick et al., 2004); the traditionally used wavelengths do not yield good results. Hence, we utilized the longer wavelength bands (743 and 835 nm) in SSC retrieval using AWSS.

The evolved AWSS is expected to have advantageous properties such as insensitivity to intensity variations and precise absorption position matching. This property of AWSS is very useful in classifying the pixels with varied SSC concentrations ranging from a few tens of ppm to several thousands of ppm. Comparison of results estimated by TSM, SSMR, and AWSS (Fig. 4) indicates that the TSM algorithm could at the most discriminate only two SSC classes ranging between 0 and 1000 ppm. The SSMR algorithm could classify four major classes of SSC within 500 to 2000 ppm range. Values lower than 500 and higher than 2000 ppm could not be classified by this approach. Whereas, the AWSS could classify the image into 11 distinct SSC classes with values ranging from <500 ppm to >5000 ppm. This is mainly attributed to incorporation of longer wavelength bands in the analyses and efficacy of SAM and SFF. The accuracy of SSC estimation by this approach matches well (R^2 = 0.95 at 99% significance levels) with the field measured values.

To estimate the effects of mineralogy, reflectance at 743 and 835 nm was compared across different estuarine waters for a constant SSC value. It is evident from Fig. 3(a and b) that the convex hull normalized reflectance (at each of the tested sediment concentrations) of Narmada, Mahi and Gulf waters correlates well (R^2 = 0.94–0.97). This observation indicates that in the study area composition of suspended sediments does not influence the reflectance of water significantly. Similarly, comparison between Purna waters (with sandy sediments) and Gulf, Narmada, and Mahi waters (with silt and clayey sediments) also yielded reasonably good correlation (R^2 = 0.71–0.78) (Fig. 3c). These two observations indicate that in Gulf of Cambay, sediment concentration is the single most influential variable affecting the reflectance of water. Lesser influence of sediment size on water reflectance could be attributed to reduced effect of grain size at very high sediment concentrations. The following conclusions emerge from this study:

(i) Spectral similarity based AWSS is more effective in classifying the high turbid waters than the band ratio based approaches such as TSM and SSMR.
(ii) Reflectance in longer wavelength regions (743 and 835 nm) is more sensitive to SSC changes in Case-2 waters. Hence, spectral similarity based approach involving all OCM bands are more advantageous than using the visible bands alone.

Table 1
Mineralogy and grain size distribution of suspended sediments collected in estuaries and Gulf.

Mahi estuary		Narmada estuary		Purna estuary		Gulf of Cambay	
Grain size distribution[α] (wt.%)	Mineralogy	Grain size distribution[β] (wt.%)	Mineralogy	Grain size distribution[γ] (wt.%)	Mineralogy	Grain size distribution[δ] (wt.%)	Mineralogy
Fine sand (7–9) Silt (56–71) Clay (12–22) Organic matter (2.2–2.4) [α]Min–max ranges for 7 samples	Quartz, feldspar, muscovite, kaolinite, calcite, montmorillonite	Fine sand (11–33) Silt (63–72) Clay (3–16) Organic matter (2.5–3.3) [β]Min–max ranges for 10 samples	Quartz, feldspar, muscovite, calcite, montmorillonite	Sand (2–10) Silt (80–82) Clay (4–14) Organic matter (2.9–3.4) [γ]Min–max ranges for 4 samples	Quartz, feldspar, chlorite, kaolinite, montmorillonite	Fine sand (2–3) Silt (49–75) Clay (12–32) Organic matter (3–3.5) [δ]Min–max ranges for 12 samples	Quartz, feldspar, muscovite, kaolinite, calcite, kaolinite, chlorite, gypsum, aragonite, montmorillonite

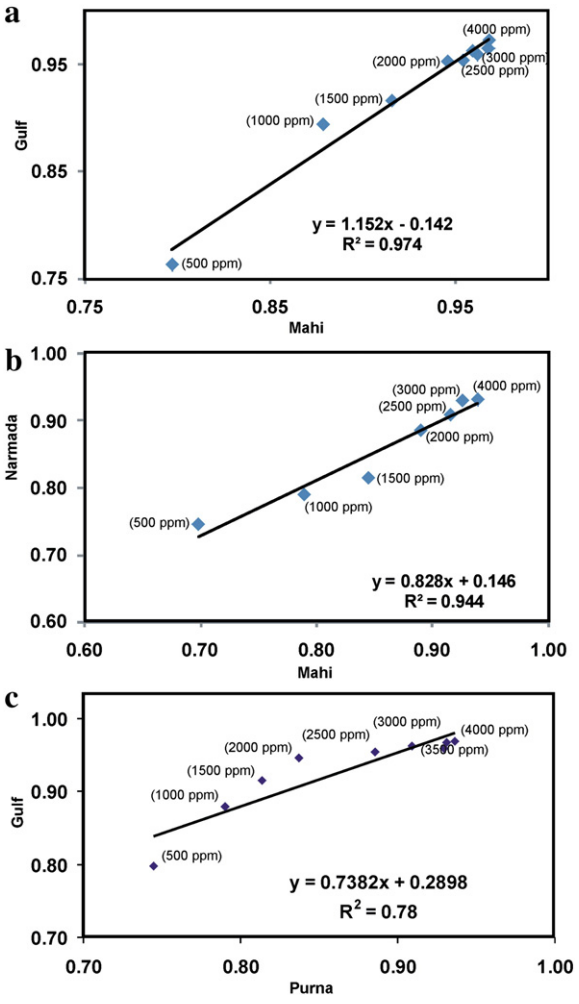

Fig. 3. Correlation of reflectance values at 740 nm between Mahi and Gulf waters (a), Narmada and Mahi waters (b), Gulf and Purna waters (c) at various sediment concentrations.

(iii) In the Gulf of Cambay, the SSC is the most important variable influencing the reflectance of estuarine and Gulf waters.

Since this study is nonspecific and aims at establishing relationship between sediment parameters and coastal water reflectance, the proposed methodology has tremendous application potential for estimating suspended sediment concentration in any coastal environment.

Table 2
Spectral similarity scores between field and laboratory spectra at different SSCs.

SSC–field measured (ppm)	SSC–lab measured (ppm)	SSC–OCM derived (ppm)	Spectral similarity measure			
			SAM	SFF	BE	AWSS
Gulf						
1600	2000	1500	0.92	0.99	0.80	0.89
2600	2500	2500	0.94	0.99	0.81	0.91
4905	4000	4500	0.92	0.99	0.83	0.90
757	1000	1000	0.93	0.99	0.86	0.96
Mahi						
1325	1500	1500	0.90	0.99	0.93	0.93
3754	4000	3500	0.84	0.98	0.83	0.88
Narmada						
3712	4000	3500	0.92	0.99	0.83	0.90
4000	5000	4000	0.95	0.99	0.86	0.92
5312	5500	5000	0.94	0.99	0.90	0.93

Acknowledgments

D.R. acknowledges both anonymous reviewers and Prof. John T. Wells for their comments that were very useful in improving the quality of the paper.

References

Carrol, D., 1970. Clay minerals: a guide to X ray diffraction. Geological Society America Special Paper 125, 85–90.

Chauhan, O.S., Rajawat, A.S., Pradhan, Y., Suneethi, J., Nayak, S.R., 2005. Weekly observations on dispersal and sink pathways of the terrigenous flux of the Ganga–Brahmaputra in the Bay of Bengal during NE monsoon. Deep-Sea Research II 52, 2018–2030.

Chen, Z.Q., Hu, C.M., Frank, M.K., 2007. Monitoring turbidity in Tampa Bay using MODIS/Aqua 250 m imagery. Remote Sensing of Environment 109 (2), 207–220.

Clark, R.N., Gallagher, A.J., Swayze, G.A., 1990. Material absorption band depth mapping of imaging spectrometer data using the complete band shape least-squares algorithm simultaneously fit to multiple spectral features from multiple materials. Proceedings of the Third Airborne Visible/Infrared Imaging Spectrometer (AVIRIS) Workshop JPL Publication, 90–54, pp. 176–186.

Dekker, A.G., Vos, R.J., Peters, S.W., 2001. Comparison of remote sensing data, model results and in situ data for total suspended matter (TSM) in the southern Frisian lakes. Science of the Total Environment 268 (1), 197–214.

Deng, M., Li, Y., 2003. Use of SeaWiFS imagery to detect three-dimensional distribution of suspended sediment. International Journal of Remote Sensing 24 (3), 519–534.

Doerffer, R., Fischer, J., 1994. Concentrations of chlorophyll, suspended matter, and Gelb–Stoff in Case-2 waters derived from satellite coastal zone color scanner data with inverse modeling methods. Journal of Geophysical Research 99, 7457–7466.

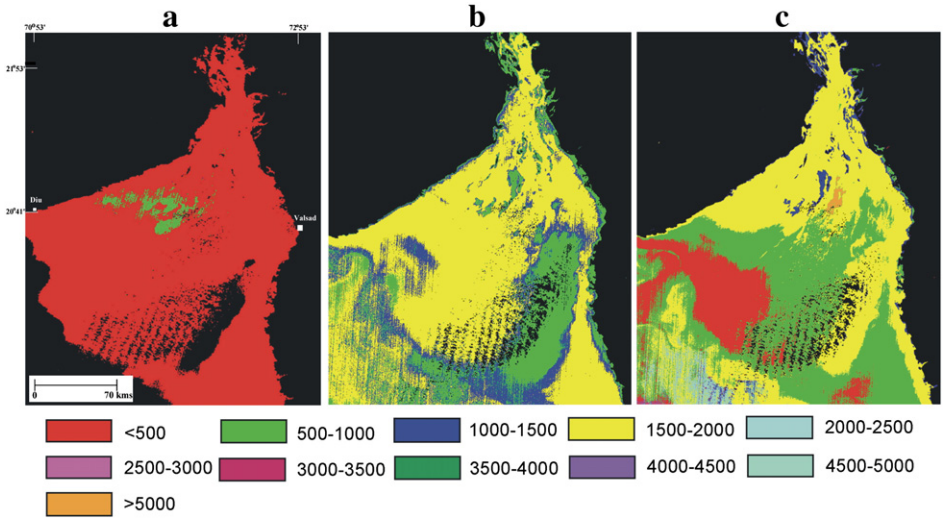

Fig. 4. Classified OCM images, depicting the SSC ranges (values in ppm) generated using TSM (a), SSMR (b), and AWSS (c) algorithms.

Doxaran, D., Froidefond, J.M., Lavender, S., Castaing, P., 2002. Spectral signature of highly turbid waters application with SPOT data to quantify suspended particulate matter concentrations. Remote Sensing of Environment 81, 149–161.

Forget, P., Ouillon, S., 1998. Surface suspended matter off the Rhone river mouth from visible satellite imagery. Oceanologica Acta 21 (6), 739–749.

Green, A.A., Berman, M., Switzer, P., Craig, M.D., 1988. A transformation for ordering multi-spectral data in terms of image quality with implications for noise removal. IEEE Transactions on Geoscience and Remote Sensing 26 (1), 65–74.

Han, Z., Jin, Y.Q., Yun, C.X., 2006. Suspended sediment concentrations in the Yangtze River estuary retrieved from the CMODIS data. International Journal of Remote Sensing 27 (19), 4329–4336.

Jervis, T.B., 1838. Additional observations on the remarkable tides in the Gulf of Cambay. Journal of the Royal Geographical Society of London 8, 202–205.

Kruse, F.A., Lefkoff, A.B., Boardman, J.B., Heidebrecht, K.B., Shapiro, A.T., Barloon, P.J., Goetz, A.F.H., 1993. The spectral image processing system (SIPS) — interactive visualization and analysis of imaging spectrometer data. Remote Sensing of the Environment 44, 145–163.

Kunte, P.D., 2008. Sediment concentration and bed form structures of Gulf of Cambay from remote sensing. International Journal of Remote Sensing 29 (8), 2169–2182.

Lira, J., Morales, J., Zamora, F., 1997. Study of sediment distribution in the area of the PaÂ nuco river plume by means of remote sensing. International Journal of Remote Sensing 18 (1), 171–182.

Mazer, A.S., Martin, M., Lee, M., Solomon, J.E., 1988. Image processing software for imaging spectrometry data analysis. Remote Sensing of Environment 24, 201–210.

Miller, R.L., McKee, B.A., 2004. Using MODIS Terra 250 m imagery to map concentration of total suspended matter in coastal waters. Remote Sensing of Environment 93 (1), 259–266.

Mobley, C.D., 1999. Estimation of the remote-sensing reflectance from above-surface measure-ments. Applied Optics 38, 7442–7455.

Mohan, M., Chauhan, P., 2003. Atmospheric correction for ocean color remote sensing. IRS-P4 OCM/Satcore project report, 1 1–5.

Nambiar, A.R., Rajagopalan, G., 1995. Radiocarbon dates of sediment cores from inner continental shelf off Taingapatnam, southwest coast of India. Current Science 68 (11), 1133–1137.

Novo, E.M.M., Hansom, J.D., Curran, P.J., 1989. The effect of viewing geometry and wave-length on the relationship between reflectance and suspended sediment concentration. International Journal of Remote Sensing 10 (8), 1357–1372.

Pollack, J.B., Cuzzi, J.N., 1980. Scattering by non-spherical particles of size comparable to wavelength: a new semi-empirical theory. In: Schuerman, D.W. (Ed.), Light Scattering by Irregularly Shaped Particles. Plenum publication, New York, pp. 113–125.

Ramakrishnan, D., Kusuma, K.N., Bharti, Rishikesh, Das, M., 2012. Relevance of spectroscopic approach in the retrieval of suspended sediment concentration (SSC) in Case-2 waters: an investigation in the high turbid waters of Gulf of Cambay, India. IEEE International Geoscience and Remote Sensing Symposium (IGARSS), Munich, Germany, pp. 4833–4836.

Ramaswamy, V., Rao, P.S., Thwin, S., Rao, N.S., Raiker, V., 2004. Tidal influence on suspended sediment distribution and dispersal in the northern Andaman Sea and Gulf of Martaban. Marine Geology 208 (1), 33–42.

Sathyendranath, S., Prieur, L., Morel, A., 1989. A three component model of ocean colour and its application to remote sensing of phytoplankton pigments in coastal water. International Journal of Remote Sensing 10, 1373–1394.

Tassan, S., 1993. An improved in-water algorithm for the determination of chlorophyll and suspended sediment concentration from Thematic Mapper data in coastal waters. International Journal of Remote Sensing 14 (6), 1221–1229.

Unnikrishnan, A.S., Shetye, S.R., Michael, G.S., 1999. Tidal propagation in the Gulf of Kham-bhat, Bombay High and surrounding areas. Proceedings of the Indian Academy of Sciences (Earth and Planetary Science) 108, 155–177.

Warrick, J.A., Mertes, L.A.K., Siegel, D.A., Mackenzie, C., 2004. Estimating suspended sediment concentrations in turbid coastal waters of the Santa Barbara Channel with SeaWiFS. International Journal of Remote Sensing 25 (10), 1995–2002.

Yanjiao, W., Feng, Y., Peiqun, Z., Wenjie, D., 2007. Experimental research on quantitative inversion models of suspended sediment concentration using remote sensing technology. Chinese Geographical Science 17 (3), 243–249.